Formation of zonal band structure in forced two-dimensional turbulence on a rotating sphere

Toru Nozawa[a] and Shigeo Yoden[b]
Department of Geophysics, Kyoto University, Kyoto 606-01, Japan

(Received 20 May 1996; accepted 24 March 1997)

A series of numerical experiments on the forced two-dimensional turbulence on a rotating sphere were done to investigate the formation processes of zonal band structures and their sensitivity to two experimental parameters of the rotation rate and the forcing wave number. A high-resolution barotropic full spherical model of T199 truncation is used with a homogeneous and isotropic formulation of the vorticity forcing function. Three different flow regimes are obtained and one of them is a new regime previously unknown. In the cases of no rotation, a very large flow pattern is obtained as a result of the upward energy cascade to the lowest wave number. The pattern irregularly fluctuates with time. A zonal band structure that consists of alternating easterly and westerly jets becomes dominant with an increase in the rotation rate. The alternating jets, which are robust and persistent, are already formed to be discernible in the very early stage of the time integration. The width of the jets decrease and the number of those increases as the rotation rate increases. The upward cascade of the disturbance energy ceases owing to the effect of rotation around a characteristic wave number n_β at which the ''β term'' is comparable to the nonlinear Jacobian term. Scale separation between the scale of cascade arrest and the forcing scale allows a systematic alignment of the vortices elongated by the shear in the zonal mean zonal flow, and such an alignment maintains the zonal band structure. When the forcing wave number is small and the rotation rate is large, the band structure is confined in high latitudes yielding a circumpolar vortex with a strong easterly jet, and a wavy structure dominates in middle and low latitudes. This is the new flow regime that is found in this study. Any systematic phase relation is not established in these latitudes because the phases are scrambled by the forcing due to the insufficient scale separation, therefore, the alternating zonal band structure does not emerge. [S1070-6631(97)02107-7]

I. INTRODUCTION

For two-dimensional (2-D) turbulence on an infinite plane, Kraichnan[1] and Leith[2] theoretically predicted the energy spectrum that has two power laws of k^{-3} in the normal enstrophy-cascading range and of $k^{-5/3}$ in the upward energy-cascading range. Since then many numerical experiments have been done to examine several aspects of the 2-D turbulence theory.[3–5] One of the most remarkable features of the flow field obtained in the numerical experiments is the emergence of isolated coherent vortices in decaying 2-D turbulence.[6] Characteristics of these coherent vortices have been investigated in detail using a surprisingly high-resolution model with 1024^2 grids.[7]

A geophysical application of the 2-D turbulence theory was first done by Rhines[8] with a numerical model on a β plane to investigate the effect of the rotation of planets on the 2-D turbulence. He showed that the upward energy cascade ceases roughly at a characteristic wave number $k_\beta = \sqrt{\beta/2U}$, where U is the rms velocity and β the meridional gradient of the Coriolis parameter f. The conversion from turbulence into Rossby waves takes place around the wave number k_β. He also found that the flow field becomes anisotropic and a zonal band structure that consists of alternating easterly and westerly jets emerges owing to the β effect. Another numerical experiment on decaying 2-D turbulence on a β plane was performed by Holloway and Hendershott[9] to investigate the validity of their closure model, which is an extension of the turbulence ''test-field model'' proposed by Kraichnan.[10] They showed that the flow field has a strong zonal anisotropy in the range of $k \lesssim k_\beta^H \equiv \beta/Z$, where Z is the rms vorticity. Later, Shepherd[11] numerically studied the 2-D turbulence on a β plane under the existence of an imposed large-scale zonal jet. He showed that the disturbance energy is transferred into the range of $k \lesssim k_\beta$ owing to the shear-induced spectral transfer, and that the disturbance flow field becomes meridionally anisotropic in this low-wave number range.

Maltrud and Vallis[12] numerically studied the forced 2-D turbulence on a β plane with a high-resolution model (256^2 or 512^2 grids) under recent advanced computing facilities. In their experiments, coherent vortices become weak while anisotropy of the flow field increases as the strength of the β effect increases. Moreover, Vallis and Maltrud[13] showed that the obtained zonal band structure is extremely robust and persistent, and that the meridional scale of the obtained zonal jets becomes small as the strength of the β effect increases. A similar zonal band structure was also found in the numerical experiment on a quasigeostrophic two-layer β-plane turbulence[14] forced by an imposed unstable vertical shear. In

[a]Corresponding author. Current address: Disaster Prevention Research Institute, Kyoto University, Kyoto 611, Japan. Telephone: +81-774-38-4159; Fax: +81-774-33-0026; Electronic mail: nozawa @bouhuu.dpri.kyoto-u.ac.jp
[b]Electronic mail: yoden@kugi.kyoto-u.ac.jp

these experiments, the westerly jets are narrower and sharper than the easterly ones. This asymmetry between the westerly and the easterly jets has been studied and discussed by Marcus and Lee.[15] A recent review on the basic dynamics of jets was given by Rhines.[16]

The nature of the 2-D turbulence in spherical geometry is interesting because of the finiteness of the domain without any artificial lateral boundary, in addition to a possible application to planetary atmospheres. Williams[17] did a series of numerical experiments on the forced 2-D turbulence on a rotating sphere, and he reproduced a zonal band structure similar to that of Jovian atmosphere for experimental conditions appropriate to Jupiter. However, the computational domain was restricted to $\frac{1}{16}$ of the entire sphere under the assumptions of longitudinal periodicity and equatorial symmetry, and the forcing function he adopted was not isotropic. Hence, the obtained band structure in the flow field might be influenced by the assumed boundary conditions and the anisotropic vorticity forcing. Another numerical experiment on the forced 2-D turbulence on a rotating sphere was done by Basdevant *et al.*[18] to investigate the predictability properties of the flow field. In their experiments, however, the obtained flow field did not show such a strong zonality as that of Williams.[17]

A few years ago, Yoden and Yamada[19] did a series of numerical experiments on the decaying 2-D turbulence on a rotating sphere to investigate the effects of rotation and sphericity. They found an easterly jet in high latitudes for large rotation rates under the existence of Rossby waves. The initial flow in their experiments has a maximum of energy spectrum at a relatively low wave number $n=10$ compared with that of the forcing ($n\sim 50$) used by Williams,[17] so that the energy transfer in their decaying turbulence may be largely different from that in Williams' forced turbulence. Recently, Cho and Polvani[20] did a series of numerical experiments on a shallow-water decaying turbulence on a rotating sphere. They obtained zonal band structure with strong easterly flow in the equatorial region, and this equatorial jet becomes strong as the Rossby deformation radius decreases.

In this paper, we perform a series of numerical experiments on the forced 2-D turbulence on a rotating sphere. On the subject of the forced 2-D turbulence in the spherical geometry, there has been no study aiming at a sweep in parameter space. Hence, this is the first step to investigate the sensitivity of the formation process of zonal band structure to the rotation rate and the forcing wave number. The model and experimental procedure are described in Sec. II; the framework of the experiment is close to that of Williams,[17] but the numerical simulation is done in a full spherical domain and a homogeneous and isotropic formulation of the vorticity forcing function is used. Results are given in Sec. III, where the obtained fluid motion is categorized into three groups and one of them is found to be a new flow regime. A discussion is presented in Sec. IV, and conclusions are presented in Sec. V.

II. MODEL AND NUMERICAL EXPERIMENT

A. Model description

Two-dimensional nondivergent flow on a rotating sphere is governed by a vorticity equation:

$$\frac{\partial \zeta}{\partial t}+\frac{1}{a^2}J(\psi,\zeta)+\frac{2\Omega}{a^2}\frac{\partial \psi}{\partial \lambda}=F+\nu\left(\nabla^2+\frac{2}{a^2}\right)\zeta, \tag{1}$$

where $\psi(\lambda,\mu,t)$ is a streamfunction field, $\zeta(\lambda,\mu,t)=\nabla^2\psi$: vorticity, λ: longitude, μ: sine latitude, t: time, ∇^2: horizontal Laplacian, $J(\psi,\zeta)$: horizontal Jacobian, a: radius of the sphere, Ω: rotation rate of the sphere, ν: kinematic viscosity coefficient, and $F(\lambda,\mu,t)$: vorticity forcing function. The second term of the viscosity term (i.e., $2/a^2$) is necessary to satisfy the conservation law of the total angular momentum.

For the forcing function F, a random Markovian formulation is used as in Lilly[3] and Williams:[17]

$$F(\lambda,\mu,j\Delta t)=RF(\lambda,\mu,(j-1)\Delta t)+\sqrt{1-R^2}\hat{F}(\lambda,\mu,j\Delta t), \tag{2}$$

where R is a dimensionless memory coefficient ($R=0.98$ as in Williams[17]), and $\hat{F}$ is a randomly generated vorticity source at every time step. The random vorticity source function is as follows:

$$\hat{F}(\lambda,\mu,j\Delta t)=\sum_{n=n_f-\Delta n}^{n_f+\Delta n}\sum_{\substack{m=-n\\ m\neq 0}}^{n}\hat{F}_n^m(j)Y_n^m(\lambda,\mu), \tag{3}$$

where $\hat{F}_n^m(j)$ is an expansion coefficient of $\hat{F}$ with spherical harmonics $Y_n^m(\lambda,\mu)$. We set the amplitude and phase of the coefficients randomly at every time step j in order to construct a homogeneous and isotropic forcing. The forcing is given in a narrow range between $n_f-\Delta n$ and $n_f+\Delta n$ with $\Delta n=2$, and the rms amplitude is held constant to $\|F\|\equiv\sqrt{\langle\hat{F}^2\rangle}$ in each run, where $\langle\cdots\rangle$ denotes the spherical average. Figure 1 shows an example of the forcing field at a particular time step with $n_f=40$.

The vorticity equation (1) can be nondimensionalized by taking the radius of the sphere as a length scale and the reciprocal of the rotation rate of the sphere as a time scale:

$$\frac{\partial \zeta_*}{\partial t_*}+J(\psi_*,\zeta_*)+2\frac{\partial \psi_*}{\partial \lambda}=\alpha_E^{-1}F_*+\mathrm{Re}_E^{-1}(\nabla_*^2+2)\zeta_*, \tag{4}$$

where the subscript $*$ denotes that the quantity is nondimensional, and $\alpha_E\equiv\Omega^2/\|F\|$ and $\mathrm{Re}_E\equiv\Omega a^2/\nu$ are two dimensionless numbers. Note that the forcing function F is nondimensionalized as $F_*=\|F\|^{-1}F$. Equation (4) means that the flow that has the same values of (α_E,Re_E) is dynamically similar if the forcing wave number is unchanged in Eq. (3).

In Eq. (1), thus in Eq. (4), any sort of large-scale dissipation is not introduced because such a dissipation may affect the dynamics in undesired ways. The main problem with not using any large-scale dissipation is that a final equilibrium state can be hardly reached. The equilibrium state might be reached in the spherical geometry because it is a closed domain. However, it requires very hard computations

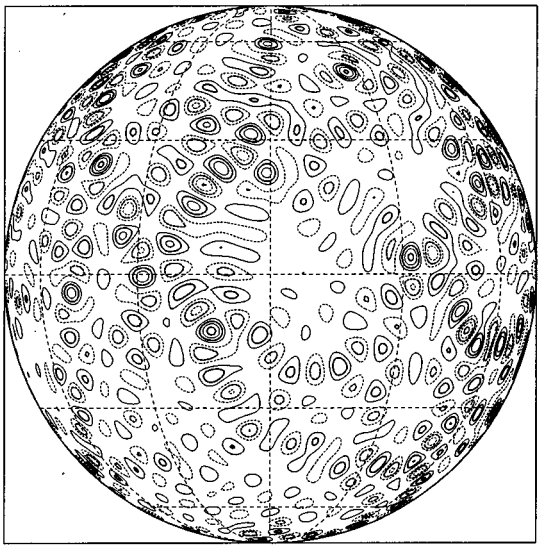

FIG. 1. Vorticity forcing field at $t=100$ J.days with $n_f=40$. The contour interval is 2.5×10^{-11} s^{-2} and negative areas are denoted by dotted lines. The zero contour has been deleted. Orthographic projection is used with the center at $\lambda=0°$ and $\varphi=0°$. Meridians and parallels are drawn for every 30°.

to achieve the equilibrium state, so that it is practically impossible with the state of the art computing facilities.

B. Numerical experiment

Numerical simulations are done for Eq. (1). The radius and the rotation rate of the sphere are set to those of Jupiter just for a geophysical reference; $a=7.00\times10^7$ m and $\Omega=\Omega_J=1.76\times10^{-4}$ rad s^{-1}. Time t is measured by a Jovian day; 1 J.day$=2\pi/\Omega_J=3.57\times10^4$ s. The kinematic viscosity coefficient of $\nu=5.00\times10^5$ m^2 s^{-1} is adopted as in Williams.[17] A pseudospectral method with a triangular truncation of T199 ($n\leqslant199=N$) is used for the computation of the advection (Jacobian) term; grids for the spectral transformation are 600 in longitudes and 300 in latitudes. Equation (1) is integrated from an initial condition of zero velocity field. The Runge–Kutta–Gill method is used for the time integrations with $\Delta t=0.05$ J.day. All of the computations are done in double precision.

Time integrations are halted at 1000 J.days, although the total energy at that time is not more than 5% of the estimated energy in the final equilibrium. However, the integration period of 1000 J.days is long enough for the formation of zonal bands, as will be shown in Fig. 3; the zonal band structure has already been established by that time, although the intensity of the jets continues to increase gradually. This work is fundamentally aimed at investigating the formation process of such a zonal band structure.

Table I gives a summary of 18 experiments that will be reported in this paper. We perform three series of the experiments with the forcing wave number of $n_f=20$, 40, or 79. For each forcing wave number, six values of the rotation rate are chosen: $\Omega/\Omega_J=0.00$, 0.25, 0.50, 1.00, 2.00, and 4.00. The sphere has Ω/Ω_J rotations par unit J.day. The rms amplitude of the forcing $\|F\|$ is determined by a method of trial and error to obtain a similar value of the kinetic energy averaged over the sphere ($\mathscr{E}\approx2.45\times10^3$ m^2 s^{-2}) in the cases of no rotation, and the amplitude is not changed for the runs with the same forcing wave number. Two dimensionless numbers Re_E and α_E in Eq. (4), are also listed in Table I, except for the cases without rotation, in which cases the nondimensionalization with Ω^{-1} is not appropriate in these runs. For each n_f, six points on the curve of $\alpha_E=\|F\|^{-1}(\nu/a^2)^2\,\mathrm{Re}_E^2$ are chosen for the parameter sweep. The sequence of random numbers for the vorticity source function is unchanged for all the experiments.

Table I also shows some characteristic quantities that are obtained from the flow field at 1000 J.days. The kinetic energy $\mathscr{E}$ and the enstrophy $\mathscr{Q}$ are determined internally and have different dependence on the experimental parameters

TABLE I. Summary of experiments. The column headings are given in the text.

Series	Run no.	n_f	Ω/Ω_J	$\|F\|$ (s^{-2})	Re_E	α_E	$\mathscr{E}$ (m^2 s^{-2})	$\mathscr{Q}$ (s^{-2})	Ro	Re	Group	n_β
I	1	20	0.00	7.85×10^{-12}	⋯	⋯	2.46×10^3	2.29×10^{-11}	⋯	1.45×10^3	**A**	⋯
	2		0.25		4.32×10^5	2.47×10^2	2.34×10^3	2.95×10^{-11}	3.54	1.22×10^3	**B**	5.95
	3		0.50		8.63×10^5	9.87×10^2	2.23×10^3	3.40×10^{-11}	1.94	1.08×10^3	**B**	8.51
	4		1.00		1.73×10^6	3.95×10^3	1.76×10^3	3.18×10^{-11}	1.06	8.83×10^2	**C**	12.77
	5		2.00		3.45×10^6	1.58×10^4	8.74×10^2	2.33×10^{-11}	6.44×10^{-1}	5.11×10^2	**C**	21.52
	6		4.00		6.90×10^6	6.32×10^4	3.97×10^2	1.44×10^{-11}	3.76×10^{-1}	2.96×10^2	**C**	37.06
II	7	40	0.00	2.18×10^{-11}	⋯	⋯	2.45×10^3	4.74×10^{-11}	⋯	1.01×10^3	**A**	⋯
	8		0.25		4.32×10^5	8.88×10^1	2.52×10^3	5.31×10^{-11}	4.58	9.78×10^2	**B**	5.84
	9		0.50		8.63×10^5	3.55×10^2	2.45×10^3	6.43×10^{-11}	2.55	8.65×10^2	**B**	8.31
	10		1.00		1.73×10^6	1.42×10^3	2.15×10^3	8.14×10^{-11}	1.53	6.75×10^2	**B**	12.14
	11		2.00		3.45×10^6	5.68×10^3	1.98×10^3	9.50×10^{-11}	8.63×10^{-1}	5.75×10^2	**B**	17.54
	12		4.00		6.90×10^6	2.27×10^4	1.03×10^3	7.15×10^{-11}	5.18×10^{-1}	3.46×10^2	**C**	29.18
III	13	79	0.00	7.85×10^{-11}	⋯	⋯	2.43×10^3	1.36×10^{-10}	⋯	5.89×10^2	**A**	⋯
	14		0.25		4.32×10^5	2.47×10^1	2.56×10^3	1.49×10^{-10}	7.62	5.92×10^2	**B**	5.82
	15		0.50		8.63×10^5	9.87×10^1	2.51×10^3	1.56×10^{-10}	3.93	5.68×10^2	**B**	8.27
	16		1.00		1.73×10^6	3.95×10^2	2.55×10^3	1.93×10^{-10}	2.17	5.18×10^2	**B**	11.65
	17		2.00		3.45×10^6	1.58×10^3	2.10×10^3	1.98×10^{-10}	1.21	4.22×10^2	**B**	17.29
	18		4.00		6.90×10^6	6.32×10^3	1.64×10^3	2.19×10^{-10}	7.19×10^{-1}	3.14×10^2	**B**	25.99

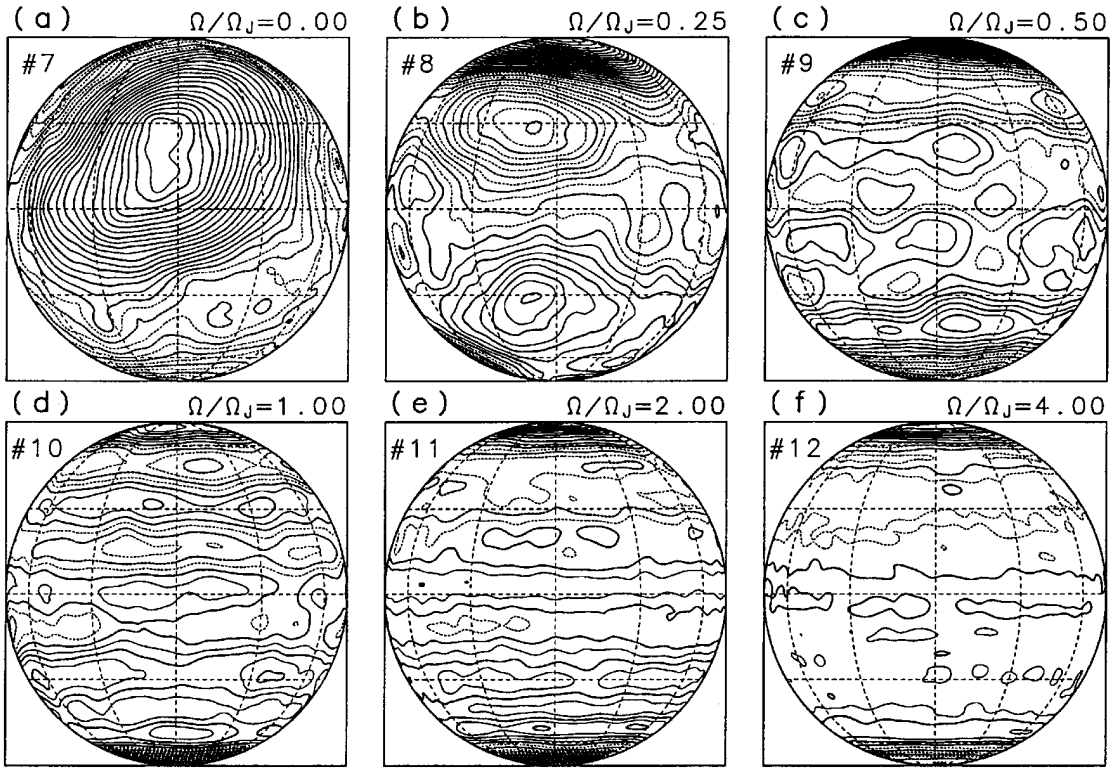

FIG. 2. The streamfunction field at $t=1000$ J.days for the runs of series II. Contour interval is 2.5×10^8 m^2 s^{-1} and negative areas are denoted by dotted lines. The map projection is the same as in Fig. 1.

n_f and Ω. From these quantities, two nondimensional numbers, Reynolds number Re and Rossby number Ro, are also defined as follows:

$$\mathrm{Re}\equiv\frac{U^\dagger L^\dagger}{\nu},\quad \mathrm{Ro}\equiv\frac{U^\dagger a}{2\Omega L^{\dagger 2}}, \tag{5}$$

where $U^\dagger$ is a velocity scale estimated as $\sqrt{2\mathscr{E}}$ and $L^\dagger$ is a length scale given by $U^\dagger T^\dagger$. Here, the time scale is estimated as $T^\dagger=1/\sqrt{2\mathscr{Q}}$. The Reynolds number Re, which is the ratio of the Jacobian term to the viscosity term in Eq. (1), is very large in the range of 300–1500, thus the role of the viscosity is not very different in all the present experiments. On the other hand, the Rossby number Ro, which is the ratio of the Jacobian term to the linear ''β term,'' varies from $\mathscr{O}(10^{-1})$ to $\mathscr{O}(1)$, except for the experiments of $\Omega=0$.

III. RESULTS

A. Formation of a zonal band structure

The streamfunction field $\psi(\lambda,\mu,t)$ at $t=1000$ J.days is shown in Fig. 2 for six values of Ω/Ω_J in the series II experiments with $n_f=40$. In the case of no rotation (a), the streamfunction field has a very large pattern that is characterized by the lowest wave number $n=2$, owing to the upward energy cascade. This flow pattern moves irregularly on the sphere without changing the pattern largely. For the experiments with rotation (b)–(f), on the other hand, zonal band structures become dominant. The zonality of the streamfunction field increases as the rotation rate increases. Although details of the flow patterns change with time, the zonal structures do not change, particularly for large rotation rates. The amplitude of ψ is large in high latitudes, forming a circumpolar vortex. The edge of the polar vortex shifts to higher latitudes as the rotation rate increases. In the rest of the streamfunction field outside of the polar vortex the amplitude of ψ decreases with an increase in the rotation rate, and the zonal band structure becomes unclear in middle and low latitudes for the most rapidly rotating case (f).

Figure 3 shows temporal variation of a zonal mean zonal angular momentum $[M]\equiv a\sqrt{1-\mu^2}[u]$ for all runs, where $u(\lambda,\mu,t)\equiv-(\sqrt{1-\mu^2}/a)(\partial\psi/\partial\mu)$ is a zonal velocity, and $[\cdots]$ denotes the zonal mean. In the cases of no rotation (#1, #7, #13; group **A**), the easterly (light blue) or westerly (dark blue) flow grows in width as the time goes by, and it dominates over a hemisphere by $t=600$ J.days or so. The easterly or westerly bands largely vary their positions with time, corresponding to the irregular movement of the large pattern of ψ, as seen in Fig. 2(a). For the cases with rotation, on the other hand, the alternating easterly and westerly zonal bands are already discernible in early stages by $t=100$ J.days or so, and do not change their positions largely after the establishment of the band structure. They become clear and robust as the rotation rate increases. These zonal band structures can be classified into two groups: one is the alternating easterly and westerly zonal band structure in all the latitudes (#2–3, #8–11, #14–18; group **B**), and the other is the circumpolar easterly jets in high latitudes and weak zonal flow in middle and low latitudes for the experiments with a small forcing wave number and a large rotation rate (#4–6, #12; group **C**). For group **B**, the number of the bands increases and their width decreases as the rotation rate increases. For large Ω(#9–11, #17–18), several mergers of westerly bands take

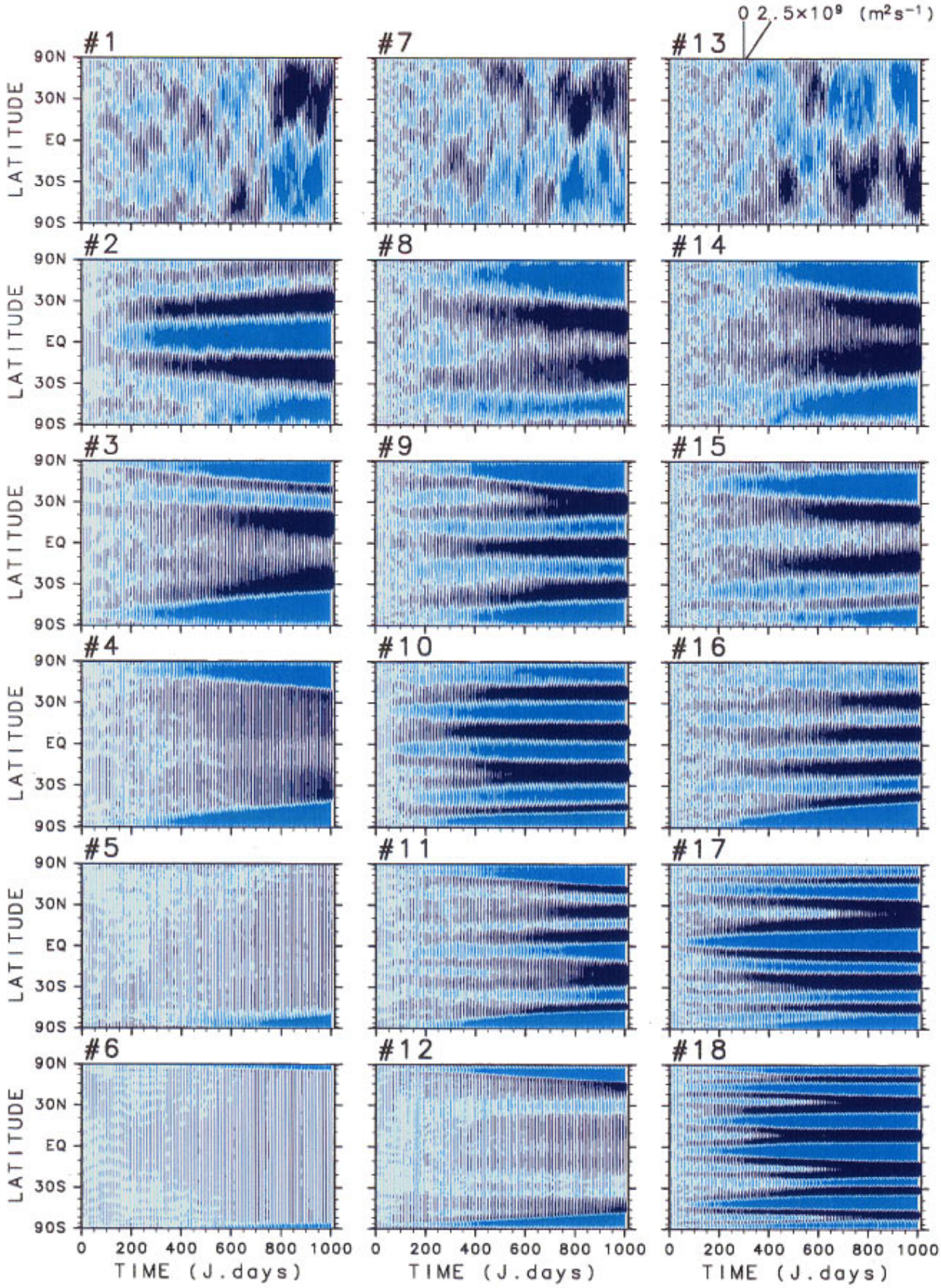

FIG. 3. Temporal variation of the zonal-mean zonal angular momentum. The time interval is 10 J.days, and the unit of an interval is 2.5×10^{9} $m^2\,s^{-1}$. Westerly zones are in dark blue while easterly zones in light. The number in the upper left of each figure represents the run number. The figures are arranged from top to bottom in the order of the rotation rate Ω/Ω_J, and from left to right in the order of the forcing wave number n_f.

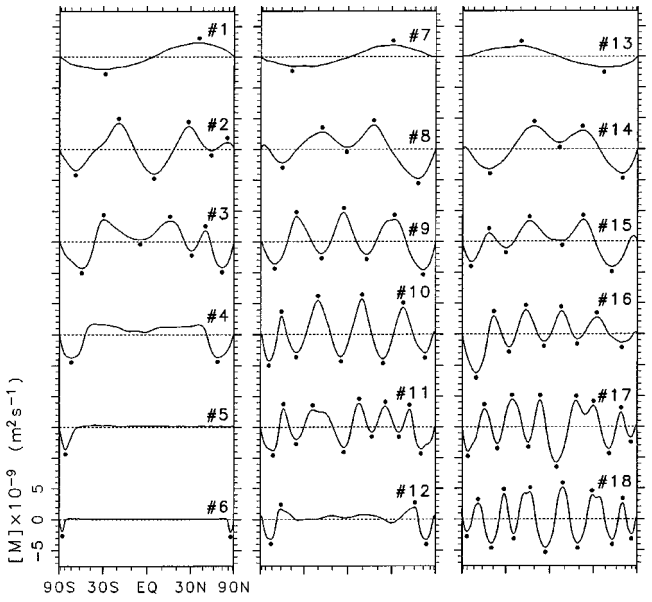

FIG. 4. Time-averaged zonal-mean zonal angular momentum for the last 200 J.days. Dashed lines are zero lines. Arrangement of the curves is identical to that of the figures in Fig. 3. Bullets are plotted above or below jet cores.

place and the width of the bands increases during such events. As the time goes by, there is a tendency that the width of easterly bands becomes broad while that of westerly becomes narrow. For group **C**, on the other hand, the position of the circumpolar easterly jets shifts to higher latitudes with an increase in the rotation rate. The width of the easterly flow becomes broad with time as in group **B**.

Figure 4 shows the meridional distribution of a time-averaged zonal mean zonal angular momentum $\overline{[M]}$, and Fig. 5 shows a curvature of the mean zonal angular momentum $\overline{[c]} \equiv \sqrt{1-\mu^2}/a \times (\partial/\partial\mu)\{(\sqrt{1-\mu^2}/a)(\partial\overline{[M]}/\partial\mu)\}$ (solid curve) and a zonal mean potential vorticity $\overline{[q]} \equiv \overline{[\zeta]} + 2\Omega\mu$ (dotted curve) for all runs, where the overbar denotes the time average from 800 to 1000 J.days. In the cases of group **A** without rotation (#1, #7, #13), the intensity of $\overline{[M]}$ is not very large and the region of the easterly or westerly flow extends over a hemisphere, as seen in Fig. 3. The curvature $\overline{[c]}$ and the zonal mean potential vorticity $\overline{[q]}$ are very small in all the latitudes. For the runs in group **B**, the intensity of the jets increases and the width of them decreases as the rotation rate increases. The curvature of the westerly flow (negative $\overline{[c]}$) is larger than that of the easterly flow (positive $\overline{[c]}$) in magnitude, and the region with negative $\overline{[c]}$ is narrower than that with positive $\overline{[c]}$. Hence, the westerly jet is narrow and steep while the easterly is broad and gentle. For the runs in group **C**, on the other hand, the intensity of the easterly jets as well as that of the westerly flows decreases as the rotation rate increases (#4–6). The magnitude of $\overline{[c]}$ is large in high latitudes while it is very small in middle and low latitudes. For the runs with rotation in group **B** and **C**, the zonal mean potential vorticity monotonously increases with μ due to the predominance of the planetary vorticity $2\Omega\mu$. The meridional gradient of $\overline{[q]}$ is, therefore, positive in all the latitudes indicating that the jets are barotropically stable.

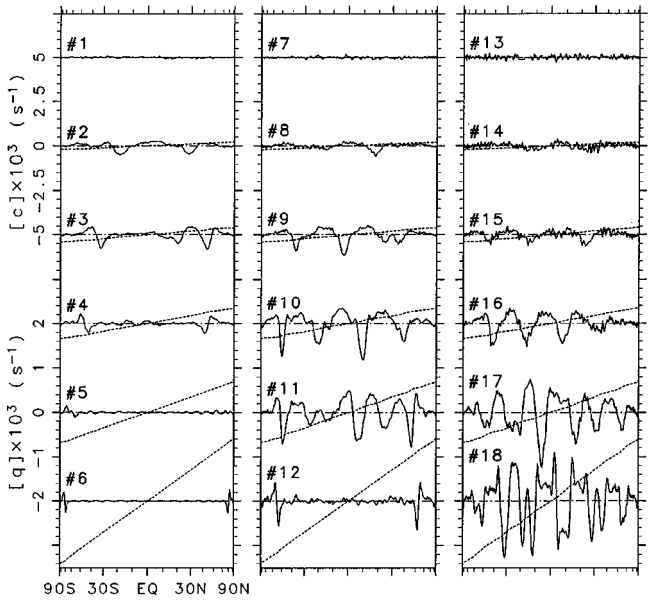

FIG. 5. Curvature of zonal-mean zonal angular momentum (solid curve) and zonal-mean potential vorticity (dotted curve) averaged from 800 to 1000 J.days. Dot–dashed lines are zero lines. Arrangement of the curves is identical to that of the figures in Fig. 3.

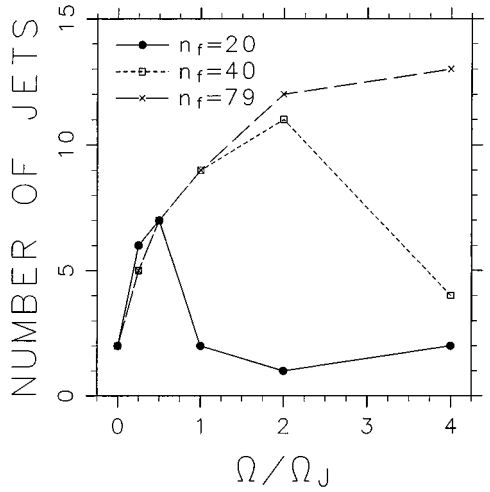

FIG. 6. Dependence of the number of jets on Ω/Ω_J for the runs of series I (solid circles connected by a solid line), for those of series II (squares connected by a dotted line), and for those of series III (×'s connected by a broken line).

In Fig. 4, we place bullets above or below the jet cores to count the number of jets in each run. The dependence of the number of jets on the rotation rate is shown in Fig. 6. As seen in Figs. 3 and 4, the number of jets increases with Ω, except for the runs in group **C**, in which the zonal-mean flow is weak in middle and low latitudes. For the experiments with the same rotation rate, the number of jets is nearly independent of the forcing wave number n_f as far as the alternating easterly and westerly jets emerge in the flow field.

Here, a characteristic wave number n_β is introduced in the analogy of Rhines' k_β:[8]

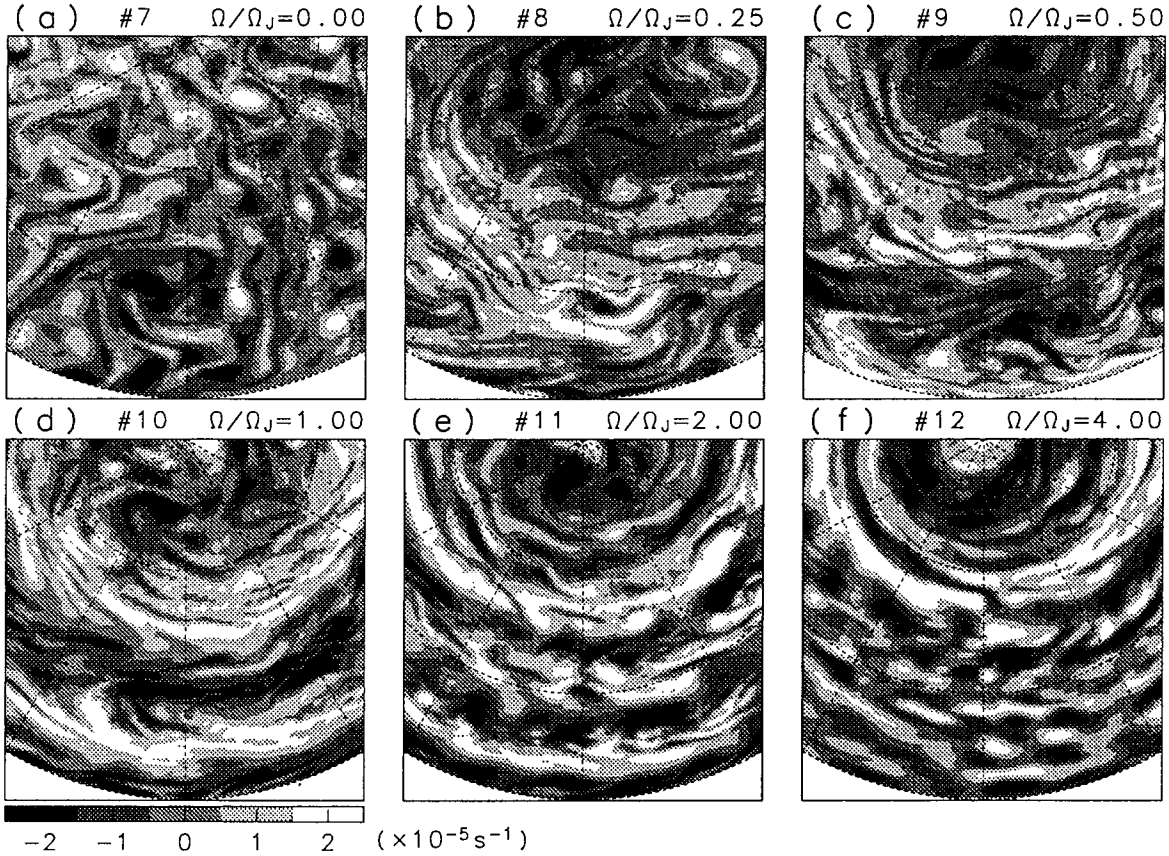

FIG. 7. Relative vorticity field at $t=1000$ J.days for the same runs as in Fig. 2. The Lambert equal area projection from the North Pole is used, and only a part of the northern hemisphere is shown. Meridians and parallels are shown for every 30°. The central meridian is identical to that in Fig. 2.

$$n_\beta(t) \equiv a\sqrt{\frac{\langle\beta\rangle}{2U(t)}}, \tag{6}$$

where $U(t)$ is the rms velocity ($U(t)=\sqrt{2\mathscr{E}(t)}$), and $\langle\beta\rangle$ is the spherical average of β: $\langle\beta\rangle=\frac{1}{2}\int_{-1}^{1}\beta\, d\mu=\pi\Omega/(2a)$. At the horizontal scale of a/n_β, the nonlinear Jacobian term is comparable to the ''β term'', $(2\Omega/a^2)(\partial\psi/\partial\lambda)$, in Eq. (1). Values of the wave number n_β at $t=1000$ J.days are listed in Table I (the last column). For the runs in group **B**, the wave number n_β at $t=1000$ J.days is small relative to the forcing wave number; $n_\beta \lesssim 0.44 n_f$. For the runs in group **C**, on the other hand, the wave number n_β is not less than $0.6n_f$.

B. Vorticity field

The relative vorticity field $\zeta(\lambda,\mu,t)$ at $t=1000$ J.days is shown in Fig. 7 for the same runs as in Fig. 2 (series II). In the case of no rotation (a), several coherent vortices emerge in the flow field, one of which corresponds to a cluster of negatively large patches near $(\lambda,\varphi)=(-10°,30°)$. A typical size of the cluster is larger than that of the forcing (see Fig. 1), suggesting some merging processes of the vorticity patches. A lot of patches of large vorticity with both signs have a rather circular structure with similar size as that of the forcing. A lot of filament structures are also seen in the rest of the vorticity field, indicating that the fluid motions are largely turbulent there. For the experiments with rotation (b)–(f), on the other hand, the pattern of the vorticity field is very different from that without rotation. When the rotation rate is small (b), the coherent vortices get elongated zonally in middle and low latitudes, although a coherent vortex can be seen in high latitudes because of the weakness of the ''β effect'' in the polar region. Patches of large vorticity are also elongated zonally in middle latitudes. In the cases with moderate rotation rate (c)–(e), the elongation takes place in all the latitudes, and the alternating positive and negative vorticity bands emerge. As the rotation rate increases, the number of the vorticity bands increases and the width of them decreases in accordance with the formation of zonal band structures. For large Ω (f) in group **C**, the vorticity band

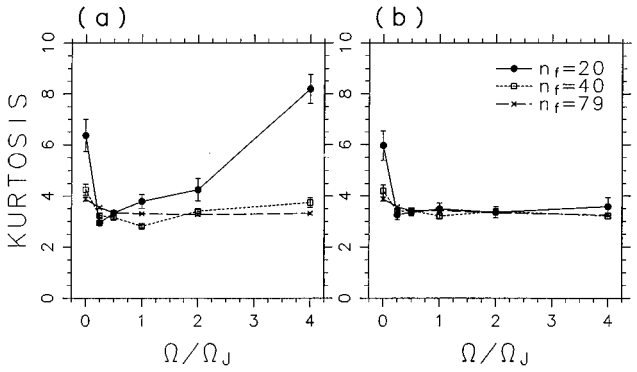

FIG. 8. Vorticity kurtosis for full components (a) and that for disturbance components (b) as functions of Ω/Ω_J. The line coding is the same as in Fig. 6. The averaged time is from 800 to 1000 J.days. Thin vertical bars indicate standard deviations for this period.

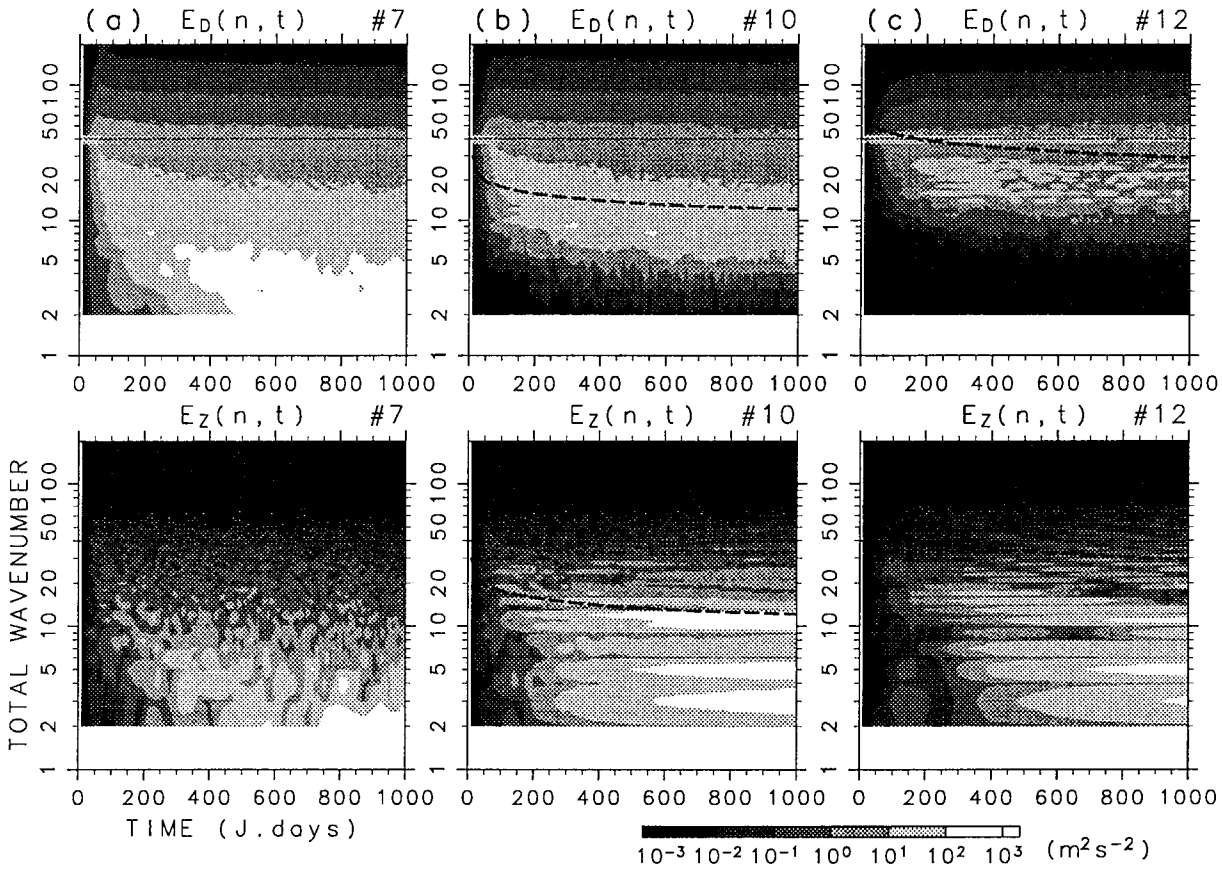

FIG. 9. Time–wave number section of energy spectra for typical three runs of #7 (a), #10 (b), and #12 (c) in series II. The upper figures show the energy spectrum for disturbances and lower ones for the zonal-mean components. The dotted lines indicate the forcing wave number ($n_f=40$) and broken curves the wave number n_β defined by Eq. (6).

structure and the elongated vortices are confined in high latitudes, whereas nearly circular vortices emerge in middle and low latitudes.

Figure 8(a) shows the dependence of time-averaged kurtosis $\overline{\mathrm{Ku}}=\overline{\langle\zeta^4\rangle/\langle\zeta^2\rangle^2}$, which is a measure of the peakedness of enstrophy (or squared vorticity) distribution, on the rotation rate for all runs. In the case with no rotation, the time-averaged kurtosis decreases with an increase in the forcing wave number n_f as shown in Maltrud and Vallis.[12] For these runs, the ratio of a dissipation wave number[21] to n_f decreases as n_f increases. Hence, it is primarily due to the dissipation effects that the time-averaged kurtosis $\overline{\mathrm{Ku}}$ decreases with an increase in n_f. For the series III experiments ($n_f=79$), the time-averaged kurtosis has the largest value in the run without rotation and it decreases as the rotation rate increases. This fact is consistent with the results of the numerical experiments on a β-plane.[12] For the series I and II experiments, on the other hand, $\overline{\mathrm{Ku}}$ is minimized for a certain value of the rotation rate ($\Omega/\Omega_J=0.25$ for $n_f=20$ and $\Omega/\Omega_J=1.00$ for $n_f=40$); for the runs with larger Ω than these thresholds, $\overline{\mathrm{Ku}}$ increases as the rotation rate increases. Figure 8(b) shows the dependence of the time-averaged kurtosis for the disturbance vorticity field defined as $\overline{\mathrm{Ku}^*}=\overline{\langle(\zeta^*)^4\rangle/\langle(\zeta^*)^2\rangle^2}$, where $(\cdots)^*\equiv(\cdots)-\overline{[\cdots]}$ denotes the disturbance field. In the cases with rotation, $\overline{\mathrm{Ku}^*}$ is nearly independent of the rotation rate as well as the forcing wave number. Hence, the increase of $\overline{\mathrm{Ku}}$ with Ω is due to the confinement of the vorticity band structure (i.e., the circumpolar vortex) to the polar region, as seen in Figs. 2 and 7.

C. Decomposition into zonal-mean and disturbance fields

In the previous section, the vorticity field is divided into the zonal-mean and disturbance fields. This kind of division is useful to investigate the formation and the maintenance of zonal band structure in detail, as reported by Shepherd.[11] The spectral energy equations for the zonal-mean and disturbance components are written as follows:

$$\frac{\partial E_Z(n,t)}{\partial t}=G_Z(n,t)+C_{DZ}(n,t)+D_Z(n,t), \tag{7}$$

$$\frac{\partial E_D(n,t)}{\partial t}=G_D(n,t)+C_{ZD}(n,t)+C_{DD}(n,t)+D_D(n,t). \tag{8}$$

Here $E_Z(n,t)$, $E_D(n,t)$: energy spectrum densities, $G_Z(n,t)$, $G_D(n,t)$: energy source functions, and $D_Z(n,t)$, $D_D(n,t)$: energy sink functions, where subscripts Z and D denote the zonal-mean and disturbance components, respectively. The energy conversion terms due to nonlinear interactions are $C_{DZ}(n,t)$, $C_{ZD}(n,t)$, and $C_{DD}(n,t)$. The term $C_{DZ}(n,t)$ is the conversion to the zonal-mean energy of n

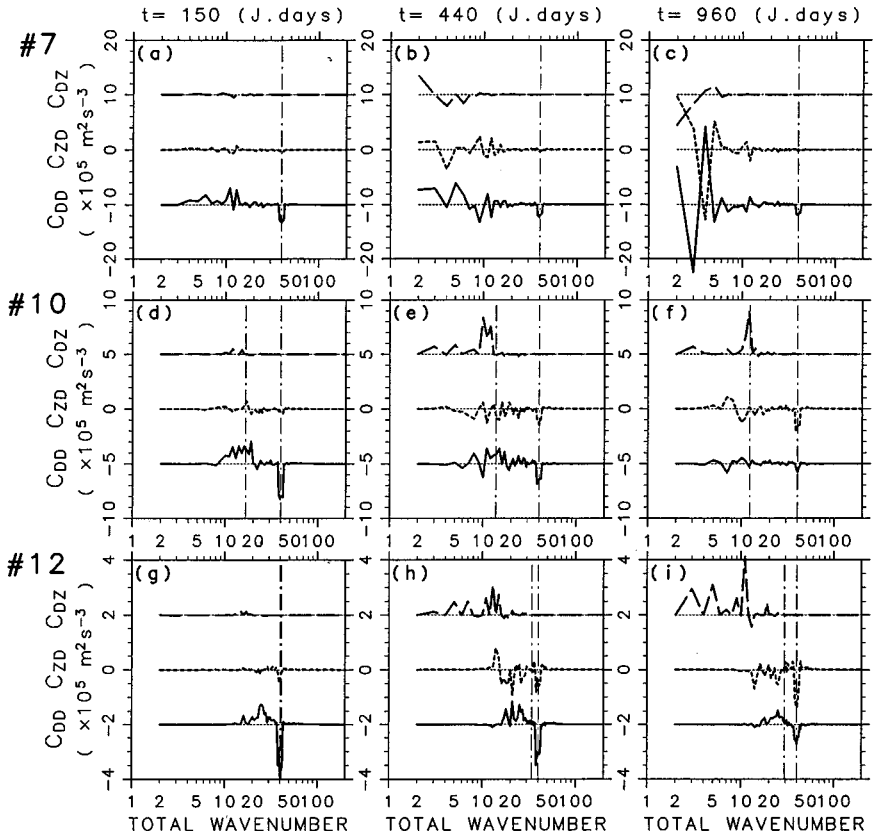

FIG. 10. Energy conversion functions averaged around $t=150$ (a), (d), (g), 440 (b), (e), (h), and 960 (c), (f), (i) J.days for the same three runs as in Fig. 9. The average is taken for 50 J.days. Thick broken, dotted, and solid lines represent $C_{DZ}(n,t)$, $C_{ZD}(n,t)$, and $C_{DD}(n,t)$, respectively. The function $C_{DD}(n,t)$ is shifted down and $C_{DZ}(n,t)$ up for clarity. Thin dotted lines are zero lines. Thin dot–dashed lines represent the wave numbers n_f and $n_\beta(t)$.

arising from the interactions between the disturbances, representing the mean zonal flow acceleration due to the meridional flux of the relative vorticity for the disturbance components ζ^*.[16] The term $C_{ZD}(n,t)$ is the conversion to the disturbance energy of n arising from the interactions between the disturbance and the zonal-mean components, representing straining of ζ^* by the shear in the zonal mean zonal flow.[11] Finally, $C_{DD}(n,t)$ is a transfer of the disturbance energy arising from the interactions (advection) between the other disturbance components. The term $C_{DD}(n,t)$ only redistributes the disturbance energy between different wave numbers, so that the sum $\Sigma_{n=2}^{N} C_{DD}(n,t)$ is always identical to zero. The explicit formulation of these terms is shown in Appendix A. Note that the energy source function for zonal components $G_Z(n,t)$ is set to be zero in this study.

Figure 9 shows time–wave number sections of $E_D(n,t)$ and $E_Z(n,t)$ for typical three runs of #7, #10, and #12 in the series II experiments. In the case of no rotation (a), the disturbance energy cascades towards the lower wave numbers as the time goes by, and the spectrum has a maximum at the lowest wave number $n=2$ by $t=600$ J.days or so. The zonal energy also cascades upward and the spectrum has a peak at $n=2$ after that time, consistent with the time evolution of $[M]$ (see Fig. 3). For the experiment in group **B** (b), on the other hand, the energy spectrum for the disturbance components has a maximum around the wave number n_β after $t\sim 200$ J.days or so, and the distribution of it does not change largely. Hence, the upward cascade of the disturbance energy ceases around n_β. The distribution of $E_Z(n,t)$ is largely different from that without rotation: the spectral components of the zonal energy, particularly in the low-wave number range of $2\leqslant n\lesssim n_\beta$, begin to increase when the disturbance energy begin to accumulate around the wave number n_β. The zonal energy increases with time at several fixed components of the spectrum, consistent with the robustness and the persistence of the meridional distribution of $[M]$, as seen in Fig. 3. For the run #12 in group **C** (c), the time evolution of $E_D(n,t)$ and $E_Z(n,t)$ is rather similar to that in #10 (b). However, the energy upward cascade for the disturbance components is hard to occur because the wave number n_β is very close to the forcing wave number n_f. Hence, $E_D(n,t)$ has a maximum around the wave number n_f for the whole integration period. The disturbance energy penetrates into the low-wave number range of $15\lesssim n \lesssim n_\beta$ and the intensity of it varies with time in this range. The number of the spectral components at which the zonal energy is dominant is larger than that in #10. Nevertheless, the number of jets in #12 is not larger than that in #10, as shown in Fig. 6. In the present case of #12, the spectral amplitude of the zonal-mean components is successfully cancelled out in middle and low latitudes by the superposition,

so that the zonal band structure does not appear there, as shown in Figs. 3 and 4.

The energy conversion terms $C_{DZ}(n,t)$, $C_{ZD}(n,t)$, and $C_{DD}(n,t)$ around three typical times of $t=150$, 440, and 960 J.days are shown in Fig. 10 for the same runs as in Fig. 9. In the case without rotation (#7), the disturbance energy forced at n_f is transferred into the lower-wave number range through $C_{DD}(n,t)$ at the beginning (a), and it reaches the lowest wavenumber $n=2$ by $t=440$ J.days (b). After the intermediate stage (b)–(c), the energy conversions between the disturbance and the zonal-mean components also take place, and they are dominant in the low-wave number range of $2\leqslant n\lesssim 7$. The direction of the energy conversion varies with time largely: from the disturbance to the zonal-mean components or *vice versa*, and this corresponds to the temporal variation of $E_Z(n,t)$ in Fig. 9(a). For the case in group **B** (#10), on the other hand, the disturbance energy forced at n_f is transferred to the wave number range around n_β, and very little energy cascades into the range of $2\leqslant n\lesssim n_\beta$ (dotted lines in (d)–(e)) as seen in Fig. 9(b). At the intermediate stage of $t=440$ J.days (e), $C_{DD}(n,t)$ is positive around n_β while $C_{ZD}(n,t)$ is negative there, indicating that the disturbance energy accumulating around n_β is converted into the zonal energy. The term $C_{DZ}(n,t)$ is positive in the range of $2\leqslant n\lesssim n_\beta$, so that the transferred energy for the disturbance components is converted to the spectral components of the zonal energy, particularly to those in the low wave number range. At this formation stage, therefore, the disturbance energy is transferred from the forcing scale to the scale of cascade arrest, and then converted to the zonal energy. At the last stage of the time integration (f), the term $C_{DD}(n,t)$ which represents the redistribution of the disturbance energy is small in all the wave number range, while the energy conversion from the disturbance to the zonal-mean components is dominant. Thus, the disturbance energy is converted to the zonal energy directly from the forcing scale at the maintenance stage. The energy conversions for the case #12 in group **C** (g)–(i) have some similar features as those for #10, but the scale separation between the scale of cascade arrest and the forcing scale is not sufficient. As a result, $C_{DD}(n,t)$ has significant values, even at the last stage of the time integration (i).

Figure 11 shows the relative vorticity field for the disturbance components ζ^* and the zonal-mean zonal angular momentum $[M]$ at $t=1000$ J.days for the same runs as in Figs. 9 and 10. In the case of no rotation (a), the disturbance vorticity field is homogeneous and isotropic. The vortex filaments are elongated in various directions insensitive to the distribution of $[M]$. For the experiment in group **B** (b), on the other hand, the disturbance vortices are elongated by the shear in the mean zonal flow in the whole sphere. This vortex elongation with systematic alignment brings the intensification of the alternating easterly and westerly zonal jets, and corresponds to the energy conversion from the disturbance to the zonal-mean components $C_{DZ}(n,t)$, as seen in Figs. 10(e) and 10(f). For the experiment in group **C** (c), the disturbance vortices have nearly circular shape in middle and low latitudes, where the shear of $[M]$ as well as the intensity of it is not very large. Thus the zonal-mean flow is not intensified. In high latitudes, on the other hand, the vortices elongated by the strong shear of $[M]$, and the circumpolar jet (or the polar vortex) is intensified.

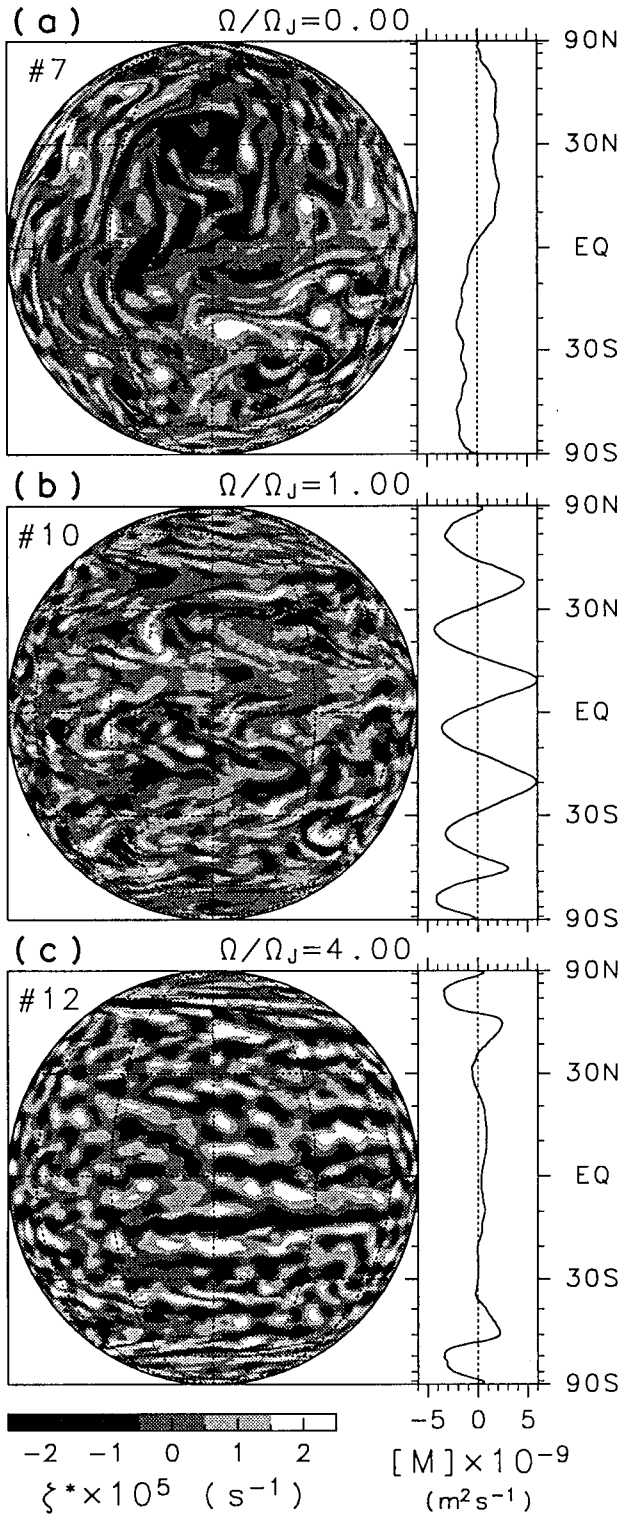

FIG. 11. Relative vorticity field for the disturbance components (left) and zonal-mean zonal angular momentum (right) at $t=1000$ J.days for the same three runs as in Figs. 9 and 10. Map projection is the same as in Fig. 1.

IV. DISCUSSION

Nearly two decades ago, Williams[17] studied the forced two-dimensional (2-D) turbulence by assuming a longitudi-

nally cyclic boundary condition and an anisotropic forcing function, and he showed an impressive clear band structure. However, the zonality of the flow field he obtained is much stronger than that obtained for similar experimental parameters using the full spherical model and the isotropic vorticity forcing function, as shown in Fig. 2(d); thus, his result is more or less influenced by his assumptions. Basdevant *et al.*[18] did a few numerical experiments on the forced 2-D turbulence on a full sphere, but they did not obtain such a clear zonal band structure as shown in Figs. 2(d) and 2(e) because of the smallness of the rotation rate and of the introduction of low-wave number dissipation.

The alternating easterly and westerly zonal band structure was found in the experiments on a quasigeostrophic two-layer β-plane turbulence,[14] as well as in the numerical experiments on a 2-D β-plane turbulence.[13] Both experiments showed that the westerly flow is narrower and sharper than the easterly. A similar difference between the westerly and the easterly flow is also seen in Figs. 3–5. This difference is a common feature both on a β-plane and on a rotating sphere. Furthermore, in Fig. 3, we can see another difference between the westerly and the easterly flows; several mergers of the westerlies take place but a merger of the easterlies does not occur in the time evolution. Prior to a westerly flow merger, easterly flows outside of the merging westerlies become wide, the westerlies become close, and then, the merging event occurs (this is clearly seen in Fig. 3, #18). Thus, the trigger of the merging process seems to be the broadening of the easterly flow, which is a characteristic effect of the disturbances in the shear flows as shown by Shepherd[11] (see his Fig. 22). The difference between the easterly and the westerly flows may be produced by meridionally propagating Rossby wave packets, which may redistribute the zonal-mean zonal angular momentum to maintain the band structure resulting in such a remarkable difference.

The zonal band structure is formed in early stages and then it becomes robust and persistent for the cases with rotation in group **B**, as shown in Fig. 3. A supplementary experiment with another random sequence for the vorticity source function (see Appendix B) shows that the band structure is quite robust after $t \sim 180$ J.days or so for a large rotation rate $\Omega/\Omega_J = 4.00$ and a large forcing wave number $n_f = 79$. However, the supplementary experiment also shows that the position of the jets largely depends on the choice of the sequence of random numbers for the vorticity source function in the very early stages, although the number of jets is nearly independent of the choice. Thus, it is difficult to predict the position of the jets.

In group **B**, vortex straining by the shear in the mean zonal flow is dominant in the whole sphere, while relatively circular vortices are dominant in middle and low latitudes in group **C** as seen in Figs. 7 and 11. This difference in the flow field between group **B** and group **C** is arised from the degree of the scale separation between the scale of cascade arrest n_β and the forcing scale n_f. For the runs in group **B**, n_β is much smaller than n_f, thus the disturbance energy can efficiently cascade toward the low-wave number range. The transferred disturbance energy accumulates around n_β with conserving a certain phase relationship; the disturbance vortices are systematically elongated by the zonal mean zonal flow. This systematic alignment intensifies the alternating easterly and westerly zonal jets.[11] On the other hand, n_β is nearly equal to or larger than n_f for the runs in group **C**, thus the effect of rotation is important even in such a small scale of the vorticity forcing. In this situation, the disturbance energy inputted around n_f is hard to cascade upward, and such a systematic phase relationship as in group **B** is not realized due to the vorticity forcing, which obliges the energy to have a random phase around n_f. This effect is enhanced by the fact that the effective n_β is even greater at low latitudes than the globally averaged value. Hence, the alternating zonal band structure is not established in the middle and low latitudes.

Yoden and Yamada[19] showed the emergence of a strong circumpolar vortex with easterly jet in the numerical experiments on decaying 2-D turbulence on a rotating sphere starting from many initial flow fields with the energy spectrum that has a maximum at a low wave number $n = 10$. The wave number n_β defined by Eq. (6) is roughly estimated to be 7.45 for their experiments with $\Omega = 100$, indicating that the scale separation between the scale of cascade arrest n_β and that of the initial flow field ($n = 10$) is insufficient. Thus the emergence of a strong circumpolar vortex with an easterly jet in their experiments may be due to the smallness of the wave number where the energy spectrum initially has a maximum.

The time integration is done only for the period of 1000 J.days, during which time the zonal band structure is sufficiently established, as seen in Fig. 3. If the simulation is performed for a very long period beyond 1000 J.days, the intensity of the zonal flow may increase gradually. Hence, the shear in the mean zonal flow may increase, and at last, a shear instability may take place. In such a situation, no one knows what happens and how the flow field is drastically changed. Further investigation on this topic will be very interesting when computing facilities become available in the future.

V. CONCLUSIONS

A series of numerical experiments on the forced 2-D turbulence on a rotating sphere were done with a high-resolution barotropic model, which has the term of homogeneous and isotropic vorticity forcing. The formation of zonal band structures in the flow field was investigated by sweeping two experimental parameters of the rotation rate and the forcing wave number, and a new flow regime was found with a small forcing wave number and large rotation rate. The process of the formation of the zonal band structure is studied by dividing the vorticity field and the spectral energy equation into the zonal-mean and disturbance components. The difference in the formation process was discussed on the basis of the degree of the scale separation between the scale of cascade arrest and the forcing scale.

In the cases of no rotation (called group **A**), the stream-function field shows a very large flow pattern that is characterized by the total wave number $n = 2$ because the energy cascades upward to the lowest wave number. The easterly or westerly flow dominates over a hemisphere and the zonal bands largely vary their positions with time, consistent with

the irregular movement of large coherent vortices in the streamfunction field. In the vorticity field, a lot of vorticity patches with circular structure are dominant, the size of which is nearly equal to that of the forcing.

For the experiments with rotation (group **B**), a zonal band structure that consists of alternating easterly and westerly jets becomes dominant in the flow field. The width of the jets decreases and the number of them increases as the rotation rate increases. The band structure is already discernible in the early stages of the time integration from the initial condition of no flow field, and it is robust and persistent for the integration period of 1000 Jovian days. The easterly jets become broad and gentle while the westerly ones become narrow and sharp. In the vorticity field, patches of large vorticity are elongated by the shear in the mean zonal flow, and the vortex elongation with systematic alignment brings the intensification of the alternating easterly and westerly zonal jets.

For the experiments with small forcing wave number and large rotation rate (group **C**), the zonal band structure is confined in high latitudes with the emergence of a circumpolar vortex with a strong easterly jet. The position of the circumpolar easterly jets shifts into high latitudes as the rotation rate increases. Outside of the polar vortex, mean zonal flow is weak westerly in middle and low latitudes, and nearly circular vorticity patches are dominant in the vorticity field.

The difference in the formation process of the zonal band structure between group **B** and group **C** may be explained as follows. For the runs in group **B**, the effect of rotation is very weak at the forcing scale, thus the inputted disturbance energy is transferred toward larger scales. The upward cascade of the disturbance energy ceases around a characteristic wave number n_β at which the ''β term'' due to planetary rotation is comparable to the nonlinear Jacobian term. The disturbance energy begins to accumulate around n_β with conserving a systematic phase relation, which corresponds to the straining of disturbance vortices by the shear in the mean zonal flow in physical space. Hence, the zonal band structure of alternating easterly and westerly jets is established and intensified by this systematic alignment of the elongated vortices. For the runs in group **C**, on the other hand, the effect of rotation is significant even at the forcing scale, thus the upward cascade of the disturbance energy hardly occurred. The phase relation of the disturbance is not systematic but scattered by the phase scrambling effect at the forcing scale. As a result, such clear zonal jets as in group **B** do not emerge in the middle and low latitudes.

ACKNOWLEDGMENTS

We thank Dr. K. Ishioka for his FORTRAN code on the pseudospectral method used in this study, and two anonymous reviewers for their useful comments. GFD-DENNOU Library was used for drawing the figures. This work was supported in part by the Grant-in-Aid from the Ministry of Education, Science, Sports, and Culture of Japan, and by the Grant-in-Aid for the Cooperative Research with the Center for Climate System Research, University of Tokyo. Computations were done in part on the KDK system at the Radio Atmospheric Science Center, Kyoto University.

APPENDIX A: DERIVATION OF THE SPECTRAL ENERGY EQUATIONS

Dividing ψ and ζ into zonal-mean and disturbance components and taking a zonal mean of the vorticity equation (1) and a deviation from that, we can obtain the following equations for the zonal-mean and disturbance vorticity:

$$\frac{\partial[\zeta]}{\partial t}+\frac{1}{a^2}[J(\psi^*,\zeta^*)] =[F]+\frac{\nu}{a^2}\left\{\frac{\partial}{\partial\mu}\left((1-\mu^2)\frac{\partial}{\partial\mu}\right)+2\right\}[\zeta], \tag{A1}$$

$$\frac{\partial\zeta^*}{\partial t}+\frac{1}{a^2}\{J([\psi],\zeta^*)+J(\psi^*,[\zeta])\}+\frac{1}{a^2}\{J(\psi^*,\zeta^*) -[J(\psi^*,\zeta^*)]\}+\frac{2\Omega}{a^2}\frac{\partial\psi^*}{\partial\lambda}=F^*+\nu\left(\nabla^2+\frac{2}{a^2}\right)\zeta^*. \tag{A2}$$

Spectral energy equations for the zonal-mean and disturbance components can be obtained by expanding each term of Eqs. (A1) and (A2) with spherical harmonics, multiplying the complex conjugate of an expansion coefficient of the streamfunction, and, for the disturbance components, summing them with respect to a zonal wave number m except for $m=0$:

$$\frac{\partial E_Z(n,t)}{\partial t}=G_Z(n,t)+C_{DZ}(n,t)+D_Z(n,t), \tag{A3}$$

$$\frac{\partial E_D(n,t)}{\partial t}=G_D(n,t)+C_{ZD}(n,t)+C_{DD}(n,t)+D_D(n,t). \tag{A4}$$

The exact representation of each term is written as follows:

$$E_Z(n,t)=\frac{1}{2}\frac{n(n+1)}{a^2}|\psi_n^0(t)|^2,$$

$$E_D(n,t)=\frac{1}{2}\sum_{\substack{m=-n\\ m\neq 0}}^{n}\frac{n(n+1)}{a^2}|\psi_n^m(t)|^2,$$

$$G_Z(n,t)=\{\psi_n^0(t)\}^\dagger F_n^0(t),$$

$$G_D(n,t)=\sum_{\substack{m=-n\\ m\neq 0}}^{n}\{\psi_n^m(t)\}^\dagger F_n^m(t)+\text{c.c.},$$

$$D_Z(n,t)=-\nu\frac{n(n+1)-2}{a^2}E_Z(n,t),$$

$$D_D(n,t)=-\nu\frac{n(n+1)-2}{a^2}E_D(n,t),$$

$$C_{DZ}(n,t)=\{\psi_n^m(t)\}^\dagger I_n^0(t),$$

$$C_{ZD}(n,t)=\sum_{\substack{m=-n\\ m\neq 0}}^{n}\{\psi_n^m(t)\}^\dagger C_n^m(t)+\text{c.c.},$$

$$C_{DD}(n,t)=\sum_{\substack{m=-n\\ m\neq 0}}^{n}\{\psi_n^m(t)\}^\dagger I_n^m(t)+\text{c.c.},$$

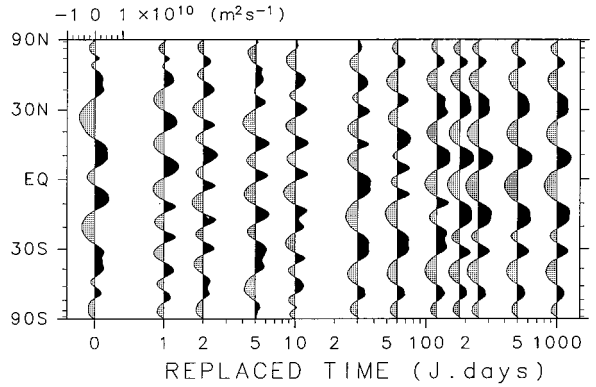

FIG. 12. Dependence of zonal-mean zonal angular momentum at $t=1000$ J.days on the replaced time t_c of the sequence of random numbers for vorticity source function (see the text). $n_f=79$, $\Omega/\Omega_J=4.00$.

where $\psi_n^m(t)$, $I_n^m(t)$, and $C_n^m(t)$ are expansion coefficients of the terms $\psi(\lambda,\mu,t)$, $(1/a^2)J(\psi^*,\zeta^*)$, and $(1/a^2)\times\{J([\psi],\zeta^*)+J(\psi^*,[\zeta])\}$, respectively:

$$\psi_n^m(t)=\frac{1}{4\pi}\int_{-1}^{1}\int_0^{2\pi}\psi(\lambda,\mu,t)\{Y_n^m(\lambda,\mu)\}^\dagger d\lambda\, d\mu,$$

$$I_n^m(t)=\frac{1}{4\pi}\int_{-1}^{1}\int_0^{2\pi}\frac{1}{a^2}J(\psi^*,\zeta^*)\{Y_n^m(\lambda,\mu)\}^\dagger d\lambda\, d\mu,$$

$$C_n^m(t)=\frac{1}{4\pi}\int_{-1}^{1}\int_0^{2\pi}\frac{1}{a^2}\{J([\psi],\zeta^*)+J(\psi^*,[\zeta])\}\times\{Y_n^m(\lambda,\mu)\}^\dagger\, d\lambda\, d\mu,$$

and, $(\cdots)^\dagger$ denotes the complex conjugate as well as the symbol c.c.

APPENDIX B: ROBUSTNESS AND PERSISTENCY OF THE BAND STRUCTURE

In order to investigate the sensitivity of the zonal band structure to the random sequences of the vorticity forcing, we perform a series of supplementary experiments for $n_f=79$ and $\Omega/\Omega_J=4.00$. A particular sequence of random numbers (denoted by $\langle 1\rangle$) was used in all the experiments stated in the main text. In this experiment the sequence of random numbers is replaced to another one ($\langle 2\rangle$) after the time t_c J.days. Figure 12 shows the dependence of the zonal-mean angular momentum at $t=1000$ J.days on the replaced time t_c. The mean zonal angular momentum at $t_c=1000$ J.days is obtained using a full random sequence of $\langle 1\rangle$, while that at $t_c=0$ J.days is obtained with a full random sequence of $\langle 2\rangle$. The positions of easterly and westerly jets are largely different depending on the random sequence, although the number of the easterly (or westerly) jets are not very different (6–8). If the sequence of random numbers $\langle 1\rangle$ is replaced after $t=180$ J.days, the mean zonal angular momentum is almost unchanged; the zonal band structure is already formed by that time and it becomes insensitive to the choice of the sequence of random numbers after that time. In high latitudes this timing is earlier than in middle and low latitudes; for example, the band structure is unchanged for $t_c\geqslant 30$ J.days in southern high latitudes. When the replaced time is very early ($t_c\leqslant 10$ J.days), on the other hand, the band structure is very sensitive to t_c.

[1] R. H. Kraichnan, ''Inertial ranges in two-dimensional turbulence,'' Phys. Fluids **10**, 1417 (1967).
[2] C. E. Leith, ''Diffusion approximation for two-dimensional turbulence,'' Phys. Fluids **11**, 671 (1968).
[3] D. K. Lilly, ''Numerical simulation of two-dimensional turbulence,'' Phys. Fluids Suppl. **12**, 240 (1969).
[4] U. Frisch and P. L. Sulem, ''Numerical simulation of the inverse cascade in two-dimensional turbulence,'' Phys. Fluids **27**, 1921 (1984).
[5] B. Legras, P. Santangelo, and R. Benzi, ''High resolution numerical experiments for forced two-dimensional turbulence,'' Europhys. Lett. **5**, 37 (1988).
[6] J. C. McWilliams, ''The emergence of isolated coherent vortices in turbulent flow,'' J. Fluid Mech. **146**, 21 (1984).
[7] P. Santangelo, R. Benzi, and B. Legras, ''The generation of vortices in high resolution, two-dimensional decaying turbulence and the influence of initial conditions on the breaking of self-similarity,'' Phys. Fluids A **1**, 1027 (1989).
[8] P. B. Rhines, ''Waves and turbulence on a beta-plane,'' J. Fluid Mech. **69**, 417 (1975).
[9] G. Holloway and M. Hendershott, ''Stochastic closure for nonlinear Rossby waves,'' J. Fluid Mech. **82**, 747 (1977).
[10] R. H. Kraichnan, ''An almost-Markovian Galilean-invariant turbulence model,'' J. Fluid Mech. **47**, 513 (1971).
[11] T. G. Shepherd, ''Rossby waves and two-dimensional turbulence in a large-scale zonal jet,'' J. Fluid Mech. **183**, 467 (1987).
[12] M. E. Maltrud and G. K. Vallis, ''Energy spectra and coherent structures in forced two-dimensional and beta-plane turbulence,'' J. Fluid Mech. **228**, 321 (1991).
[13] G. K. Vallis and M. E. Maltrud, ''Generation of mean flows and jets on a beta plane and over topography,'' J. Phys. Oceanogr. **23**, 1346 (1993).
[14] R. L. Panetta, ''Zonal jets in wide baroclinically unstable regions: Persistence and scale selection,'' J. Atmos. Sci. **50**, 2073 (1993).
[15] P. S. Marcus and C. Lee, ''Jupiter's Great Red Spot and zonal winds as a self-consistent, one-layer, quasigeostrophic flow,'' Chaos **4**, 269 (1994).
[16] P. B. Rhines, ''Jets,'' Chaos **4**, 313 (1994).
[17] G. P. Williams, ''Planetary circulations: 1. Barotropic representation of Jovian and terrestrial turbulence,'' J. Atmos. Sci. **35**, 1399 (1978).
[18] C. Basdevant, B. Legras, R. Sadourny, and M. Beland, ''A study of barotropic model flows: Intermittency, waves and predictability,'' J. Atmos. Sci. **38**, 2305 (1981).
[19] S. Yoden and M. Yamada, ''A numerical experiment on two-dimensional decaying turbulence on a rotating sphere,'' J. Atmos. Sci. **50**, 631 (1993).
[20] J. Y-K. Cho and L. M. Polvani, ''The emergence of jets and vortices in freely evolving, shallow-water turbulence on a sphere,'' Phys. Fluids **8**, 1531 (1996).
[21] G. K. Batchelor, ''Computation of the energy spectrum in homogeneous two-dimensional turbulence,'' Phys. Fluids Suppl. **12**, 233 (1969).